Wind Tunnel Measurements of Pollutant Plume Dispersion over Hypothetical Urban Areas

Ziwei Mo and Chun-Ho Liu*

Department of Mechanical Engineering, The University of Hong Kong, Hong Kong

Revised manuscript BAE-D-17-02025R1

submitted

to

Building and Environment

on

January 31, 2018

*Corresponding author address:

Chun-Ho LIU

Department of Mechanical Engineering

7/F, Haking Wong Building

The University of Hong Kong

Pokfulam Road, Hong Kong, CHINA

Tel: (852) 3917 7901

Fax: (852) 2858 5415

E-mail: liuchunho@graduate.hku.hk

Wind Tunnel Measurements of Pollutant Plume Dispersion over Hypothetical Urban Areas

Ziwei Mo and Chun-Ho Liu
Department of Mechanical Engineering, The University Hong Kong, Hong Kong
January 31, 2018

Abstract

Non-computational-fluid-dynamics (Non-CFD) solutions, such as Gaussian plume models, are commonly employed to predict ground-level pollutant concentrations because of their cost-effectiveness. Whilst, they should be applied with caution for pollutant plume dispersion over complicated urban morphology in view of their implicit limitation of empirically determined dispersion coefficients σ_z. Skin-friction coefficient c_f, which is a measure of aerodynamic resistance induced by rough surfaces, is proposed to parameterize the dispersion coefficient over urban areas in isothermal conditions. Analytical derivation shows that σ_z is proportional to the newly proposed friction length scale L_f (= $x^{1/2}$ $\delta^{1/2}$ $c_f^{1/4}$ where x and δ are the distance after pollutant source and the turbulent boundary layer thickness, respectively). Its functional form is verified by wind tunnel experiments for flows and tracer plume dispersion over hypothetical urban areas in the form of idealized street canyons of different building-height-to-street-width (aspect) ratios (ARs = 1/2, 1/4, 1/8 and 1/12). A ground-level, pollutant line source in crossflows is modeled by atomizing water vapor using ultrasonic. Ranges of turbulent boundary layer thickness (240 mm $\leq \delta \leq$ 285 mm) and skin-friction coefficient ($8\times10^{-3} \leq c_f \leq 13\times10^{-3}$) are tested. The tracer concentrations over rough surfaces exhibit the Gaussian distribution. A close correlation between σ_z and L_f is revealed (coefficient of determination R^2 = 0.93), demonstrating the influence of drag on the transport processes. The analytical solution and wind tunnel results collectively suggest an improved parameterization of pollutant plume dispersion coefficient over rough surfaces, refining the practice of the air quality forecast in urban areas. (Word count: 251)

Keywords: Aerodynamic resistance; hypothetical urban areas; pollutant plume dispersion; rough surfaces; vertical dispersion coefficient.

1. Introduction

Rapid urbanization and expanding human activities are accompanied with increasing pollutant emission and degrading air quality [1]. Roads in cities are flanked by closely packed, high-rise buildings, forming arrays of street canyons. The dynamics in the urban canopy layer (UCL) are different from those in the atmospheric boundary layer (ABL) [2]. Moreover, the drag induced by ground surfaces modifies the wind flows and the pollutant transport aloft [3,4]. Advanced understanding of the pollutant transport processes over urban areas is utmost important for public health and the formulation of pollution control strategy.

Gaussian plume model is the well-received solution to ABL pollutant dispersion because of its cost-effectiveness in air quality management [5]. Its accuracy, however, tightly depends on the functionality of dispersion coefficients (σ_y in lateral and σ_z in vertical direction). Theoretically, dispersion coefficients are functions of atmospheric turbulence and surface roughness [6,7]. Most σ_y and σ_z are empirically determined based on the atmospheric stability and the distance behind the pollutant source [8]. Whereas, the turbulence in the atmospheric surface layer (ASL) is complicated by the land feature such as natural terrain, forest vegetation or building geometry. It in turn modifies substantially the dispersion coefficients (especially σ_z), which, however, is often overlooked in the practice of pollutant plume dispersion modeling [9].

Numerous studies have been conducted to enrich our understanding of tracer transport over rough surfaces [10,11]. Reduced-scale physical modeling, such as using wind tunnels [12,13] or water channels [14,15], was one of the commonly adopted approaches. Various influential factors on pollutant dispersion, such as thermal effect [16], upstream and downstream buildings [17-19], roof-top structures [20,21], roof pitches [22] and roadway configurations (noise barriers, roadway elevation and nearby terrain) [23], were examined by wind tunnel experiments. Plume dispersion over rough surfaces was also widely investigated. Salizzoni et al. [24] compared the plume dispersion behavior over an array of (identical) roughness elements of different density together with the sensitivity to the existence of smaller roughness scales. It was found that the turbulent mass flux increased with decreasing obstacle density. Moreover, those small roughness scales further enhanced the turbulent transport processes only in the skimming flow regime (closely packed roughness elements). To study the dense-gas dispersion over rough surfaces, a series of wind tunnel experiments were conducted in three different wind tunnels in a cooperative program [25]. By monitoring the vertical concentration profiles of dense gas (carbon dioxide CO_2) and non-buoyant tracer (ethane C_2H_6) at different locations after line sources in crossflows, detailed data were archived to refine the vertical-turbulent-entrainment component of dispersion models [26,27]. Recently, Perry et al. [28] tested the tracer dispersion over elongated rectangular buildings. The vertical and lateral profiles of concentrations were measured and the Gaussian distribution was applied well in the regression. It was found that the effective plume height descended faster when the approaching flows and the buildings were inclined at 45°, suggesting that wind direction was an important factor governing the transport processes. Apart from wind tunnel experiments, mathematical modeling [29-32] and field measurements [33-35] have been deployed to investigate pollutant dispersion over different configurations of roughness elements. The aforementioned studies collectively showed that pollutant plume dispersion was closely related to surface morphology so diversified pollutant transport characteristics were unveiled over different arrangements of obstacles. Whereas, the fundamental understanding and the quantitative correlation between ASL pollutant dispersion and ground-surface roughness are rather limited.

The authors have persisted to address the aforementioned scientific questions for years. Water evaporation was employed to compare the capacity of ventilation and pollutant removal from street canyons of different building-height-to-street-width (aspect) ratios (ARs) [36]. Skin-friction coefficient c_f, as a measure of urban roughness, has been adopted for the parameterization of ventilation and pollutant removal using both numerical modelling [7,37] and wind tunnel measurements [38-40]. As an extension of our ongoing research effort, this paper looks into the flows and transport processes over hypothetical urban areas. We attempt to parameterize the vertical dispersion coefficient σ_z in the (conventional) Gaussian plume model by formulating the functional form in terms of skin-friction coefficient c_f and other flow variables. We suggest the use of Gaussian-plume framework for the concentration profiles because of its solid theoretical basis. Our hypothesis is to fine-tune the dispersion coefficient to account for the effect of urban morphology on transport processes. The theory is derived first in the next section. Afterward, wind tunnel results are reported to verify the mathematical hypothesis and to characterize the tracer plume dispersion as a function of surface roughness. This study advances our understanding of pollutant transport mechanism over cities in response to urban morphology as well as parameterizes the ASL pollutant-plume (vertical) dispersion coefficient over urban areas.

2. Theoretical background

2.1. Skin-friction coefficient

Skin-friction coefficient

$$c_f = \frac{\tau_w}{\rho U_\infty^2 / 2} = \frac{2u_*^2}{U_\infty^2}, \tag{1}$$

which is defined as the ratio of drag to (half of) dynamic pressure, is commonly used to measure the aerodynamic resistance for flows over (non-smooth) solid boundaries in the engineering community [41,42]. Here, τ_w is the shear stress induced by the rough surface, ρ the fluid density and U_∞ the freestream wind speed [7,38]. In this paper, u_* is the friction velocity estimated by extrapolating the vertical profile of turbulent momentum flux from the inertial sublayer (ISL) down to the displacement height at wall-normal distance $z = d$ [43, 44]. The ISL is defined as the region where the turbulent momentum flux is rather constant (less than 10% spatial variation in this study) [39].

2.2. Gaussian plume model

Gaussian plume dispersion model is well received by the industry to estimate ABL pollutant concentrations [8]. After a continuous, infinite line source of passive and inert pollutants in crossflows, the steady-state Gaussian plume dispersion model is

$$\psi(x,z) = \frac{Q}{\sqrt{2\pi}U\sigma_z}\left\{\exp\left[-\frac{(z-z_s)^2}{2\sigma_z^2}\right] + \exp\left[-\frac{(z+z_s)^2}{2\sigma_z^2}\right]\right\} \tag{2}$$

where ψ is (mean) pollutant concentration, U the (uniform) wind speed, z the height measuring from the ground surface, z_s the effective source height, σ_z the (vertical) dispersion coefficient and Q the pollutant emission rate. It is noteworthy that the effective source height z_s could be estimated by the best fit of Gaussian model to the measured concentrations [4]. In this paper, the emission height is essentially at the roof level so $z_s = h$ is assumed in the following analyses. It is because the flows are recirculating but not moving in the streamwise direction in-between roughness elements below the roof level. The current ground-level line source indeed would further elevate the effective source height (in the order of roughness element size h because of the discharge momentum). The related uncertainty is discussed in *Section 3.2 Source design*. The vertical profiles of pollutant concentration at any downstream positions x after the pollutant source are in the forms of Gaussian distribution characterized by the dispersion coefficient σ_z. Therefore, the reliability of σ_z is crucial to the accuracy of Gaussian plume dispersion models.

2.3. Aerodynamic resistance and plume dispersion

Dispersion coefficient σ_z is a function of ABL turbulence, surface roughness and the distance after the pollutant source [6]. It can be described by the classic K-theory, anti-gradient diffusion model, as follows

$$\sigma_z^{\,2} = 2K_z t = 2K_z \frac{x}{U} \tag{3}$$

where K_z is the eddy diffusivity in the vertical direction z and t ($= x/U$) the pollutant traveling time from the source to the receptor in the streamwise direction [45]. In the context of mixing-length theory, the eddy diffusivity can be approximated by

$$K_z \propto l_* u_* \tag{4}$$

where l_* and u_* (friction velocity) are the characteristic scales of length and velocity, respectively, of turbulent eddies. For the ground-level source, the pollutant transport is mainly governed by the near-surface turbulence so the friction velocity u_* is used as the velocity scale for the eddy diffusivity. Without loss of generality, the length scale l_* is comparable to the turbulent boundary layer thickness δ. Equation (3) is then simplified to

$$\sigma_z^2 \propto 2x\delta \frac{u_*}{U}\,. \tag{5}$$

Substituting Equation (1) $u_*/U_\infty = (c_f/2)^{1/2}$ into Equation (5) yields the basic functional form

$$\sigma_z \propto x^{1/2} \times \delta^{1/2} \times c_f^{\;1/4}\,. \tag{6}$$

Alternatively, Equation (6) can be derived from the Lagrangian approach. The (streamwise) distance traveled by advection in time t is x (= $U \times t$). By first-order approximation, the corresponding (vertical) distance traveled by diffusion is $z = (K_z \times t)^{1/2}$. The distance travel in the streamwise x and vertical z directions is therefore correlated by

$$z^2 = K_z \frac{x}{U}. \tag{7}$$

We apply the skin-friction coefficient Equation (1) and the mixing-length theory Equation (4) again, Equation (7) is simplified to $z^2 = x\, l_*\, c_f^{1/2} / 2^{1/2}$. Note that the eddy size is comparable to the turbulent boundary layer thickness $l_* \approx \delta$ and the vertical dispersion coefficient is proportional to the vertical distance traveled by pollutant $\sigma_z \propto z$, Equation (6) is thus arrived as well. Calder [46] proposed the analytical solution that $K_z = \kappa\, u_*\, z$. Hence, σ_z can be calculated as $\sigma_z^2 = 2\, K_z\, t = 2\, \kappa\, u_*\, z\, x/U$ based on Equation (3) and the height z is introduced into the calculation of dispersion coefficient σ_z. However, the functional form is different from that of conventional Gaussian models. Arya [45] used the drag coefficient to estimate K_z but the characteristic length scale l_* was not considered. Britter et al. [47] used the entrainment velocity w_e to replace u_* ($w_e = 0.65u_*$ based on wind tunnel results) while σ_z and w_e is proportional to the rate of change of vertical dispersion coefficient $w_e \propto d\sigma_z/dt$. We also tested using the size of roughness elements h to estimate the length scale but unsuccessful. Afterward. We hypothesized that the transport processes are dominated by the large-scale eddies so use the boundary layer thickness δ as the length scale, arriving the current formulation. However, our understanding of the relation between turbulence length scale l_* and the (parameterization of) dispersion coefficient σ_z is still limited. Additional studies are being undertaken to address the questions. In this paper, the analogous skin-friction coefficient and the boundary layer thickness is employed to parametrize σ_z in order to keep the conventional formulation of dispersion coefficient in terms of streamwise distance x only but not vertical distance z. It is thus proposed that dispersion coefficient can be measured by the aerodynamic resistance induced by roughness elements, which, however was not verified in the previous studies.

3. Methodology

3.1. Wind tunnel setup

Laboratory-scale experiments are performed in the open-circuit wind tunnel in the Department of Mechanical Engineering, The University of Hong Kong (Fig. 1). A honeycomb-type filter is installed upstream to suppress the (background) turbulence level due to the U-shape duct before the wind-tunnel test section. The wind-tunnel test section is 6-m long, 0.56-m wide and 0.56-m high. The design wind speed is in the range of 0.5 m sec^{-1} $\leq U \leq$ 15 m sec^{-1}. To model a turbulent boundary layer in the test section, a 2-m long upstream section is adopted on which an array of square aluminum tubes (size h = 19 mm with separation 19 mm apart) is glued (Fig. 1a). The freestream wind speed U_∞, which is measured by a Prandtl-type pitot-static tube installed upstream of the test section, is maintained at 3.3 m sec^{-1} and 6.6 m sec^{-1}, to examine the flow independence and scale similarity. The Reynolds number Re_∞ (= U_∞ δ/ ν) is calculated based on the freestream wind speed U_∞ and the turbulent boundary layer thickness δ that is in the range of 80,000 $\leq Re_\infty \leq$ 200,000. It is sufficiently high for negligible molecular viscosity effect. The wind tunnel is equipped with a traverse system for sensor positioning which is controlled by the National Instruments (NI) motion-control unit (1-mm spatial resolution). Table 1 summarizes the measurement setting employed in this study.

3.2. Source design

A ground-level line source of pollutants in crossflows is positioned in the middle of one of the street canyons. Water vapor, which is generated by an atomizer, is released as a tracer from the line source (Fig. 1b). It is driven to the ground-level line source (of width 5 mm) from a reservoir below the wind tunnel test section by an electric axial fan of constant wind speed. The amount of water vapor-moisture mixture is controlled by the power to the atomizer which is carefully adjusted to minimize the water-moisture emission in the experiments. The near-source relative humidity (RH) is sampled to ensure that it is not saturated. The flows at the exit of line source induced by the fan is w_0 (= 0.2 m sec^{-1}) which are small (3% to 6%) compared with the prevailing flows U_∞ ($\approx$ 3.3 m sec^{-1} or 6.6 m sec^{-1}) in the wind tunnel. The volumetric flux of air discharged from the line source is also small (0.1%) compared with that of the core flows in the wind tunnel. The water levels in the reservoir are the same throughout the experiments to ensure a constant emission rate of water vapor per unit length Q (= 2.4 ± 0.6 g m^{-1} sec^{-1}). In the theory of rectangular jet of unit depth, the initial plume rise induced by the discharge momentum from a line source in crossflows can be estimated by the length scales of momentum that is in order of 0.02 m to 0.04 m (h to $2h$).

3.3. Hypothetical urban models

Idealized models of urban morphology are fabricated in the form of identical street canyons using arrays of rib-type roughness elements [39]. The aluminum square tubes, whose length L is 560 mm ($L/h = 29$), span across the entire wind tunnel. They are aligned normally to the prevailing wind at separation b apart so the aspect ratio AR, which is adjustable to control the aerodynamic resistance, is equal to h/b (Fig. 1c). Four types of rough surface are considered in this paper whose ARs are 1/2, 1/4, 1/8 and 1/12, covering the skimming-flow (AR = 1/2), wake interference (AR = 1/4) and isolated roughness (AR = 1/8 and AR = 1/12) regimes [48]. This definition is analogous to the d- and k-type flows in engineering fluid mechanics [49].

3.4. Measurement techniques

The origin ($x = 0$ and $z = 0$) is set at the line source to establish the concentration grid (Fig. 1). For each measurement test, nine vertical profiles of velocity and RH are measured at selected streamwise locations in the range of $10h \leq x \leq 67.5h$ downstream of the source (Fig. S1 of the Supplementary Material). Totally 72 vertical profiles are collected in the experiments and 71 points are measured along each profile. A 20-second delay in time is applied before water vapor sampling because of the time lag of the RH sensor response.

3.4.1. Hot-wire anemometry

Velocity measurements are probed by constant-temperature hot-wire anemometer (CTA) with a X-wire probe (Fig. 1d). The sensing element of the probe consists of a pair of 5-μm (diameter) platinum-plated tungsten wires. By copper plating, the active length of the sensing element is 2 mm. The angle between two (cross) wires is 100° because a larger angle (> 90°) helps measure the elevated turbulence intensity in the near-wall region as well as reduce the errors due to inadequate yaw response in highly turbulent flows [43,49]. The analog CTA signal is digitized by a 24-bit NI data acquisition module (NI 9239). Afterward, the digital data are acquired by a desktop computer via NI CompactDAQ chassis with LabVIEW software. The sampling duration at each point is 50 sec and the sampling frequency is 2 kHz which are similar to those employed in previous studies [39,43]. A total of 100,000 velocity data are obtained at each sampling point that is sufficient for the repeatability of mean and fluctuating quantities [39]. The velocity calibration is based on the universal calibration law [50]. The freestream wind speed U_∞ data measured by CTA are also compared with those by a Pitot-static tube. Velocity calibration based on 20 points in the range of 0.5 m sec^{-1} $\leq U_\infty \leq$ 12 m sec^{-1} is conducted in prior to the wind tunnel experiments. A good correlation is observed (coefficient of determination by linear regression R^2 = 0.999) as well, demonstrating the accuracy and reliability of our CTA measurement system.

3.4.2. Humidity sensor

The RH φ and temperature T are measured by Humidity and Temperature Sensor SHT75 (SENSIRION AG Switzerland). Another SHT75 sensor is placed upstream of the water vapor source to monitor the background RH φ_0 and temperature T_0 concurrently (Fig. 1a). The RH

$$\varphi = \frac{P}{P_s} \times 100\% \tag{8}$$

is then converted to the vapor concentration (specific humidity) ψ

$$\psi = \frac{m}{V} = \frac{M \times P_s}{R_u \times (273.15 + T_0)} \times (\varphi - \varphi_0). \tag{9}$$

Here, m is the mass of water vapor (g), V the air volume (m^3), P the partial vapor pressure (Pa), P_s the saturation vapor pressure (Pa), T_0 the ambient temperature (°C), M (= 18.015 g mol^{-1}) the molar mass of water and R_u (= 8.314 Pa m^3 K^{-1} g^{-1} mol^{-1}) the universal gas constant. At each sampling point, the duration for RH measurements is 50 sec at a frequency of 1 Hz. The uncertainty of RH and T measurements is about 2% so the error in vapor concentration measurements is less than 5%.

4. Results and discussion

Flows and vapor concentration data are measured for 50 sec at each sampling point. Vertical profiles of flows are repeated in the homogeneous streamwise direction x. Hence, statistic variables are defined to facilitate analyses. In the following sections, overbar $\bar{\bullet}$, angle bracket $\langle\bullet\rangle$ and prime $\bullet'$ (= $\bullet - \langle\bar{\bullet}\rangle$) represent the temporal average, spatial average and fluctuating component, respectively, to study the dynamics. Temporal average $\bar{\bullet}$ is the averaged property during the sampling duration. Spatial average $\langle\bullet\rangle$ is the averaged property in the homogeneous streamwise direction x.

4.1. Flows

Fig. 2 depicts the vertical dimensionless profiles of mean and fluctuating velocities. Available velocity profiles from previous studies are also plotted in Fig.2 [51,52]. The velocity components are normalized by the freestream wind speed U_∞ and the vertical distance is normalized by the turbulent boundary layer thickness δ. In this paper, the turbulent boundary layer thickness is determined by the wall-normal distance where the spatio-temporal average velocity converges to 99% of the freestream wind speed $\langle\bar{u}\rangle\big|_{z=\delta} = 0.99U_\infty$. It is in the range of $12h \le \delta \le 15h$ among the cases tested in this paper (Table 1) that is comparable to that in previous studies [39,43]. The turbulent boundary layer thickness is not affected much by the freestream wind speed (about 2% difference) because of the use of identical roughness elements. Moreover, it is peaked at AR = 1/8 (δ = 285 mm).

The average velocity profiles $\langle\bar{u}\rangle$ vary only slightly over different arrays of street canyons (Fig. 2a). This indicates that the dimensionless mean profiles are not significantly affected by different configurations of surface roughness in our wind tunnel experiments and the freestream wind speed U_∞ is an appropriate characteristic velocity scale. In the ISL over non-smooth solid boundaries, the (theoretical) vertical variation of the average velocity $\langle\bar{u}\rangle$ in isothermal conditions is described by the logarithmic law of the wall (log-law) [53]

$$\langle\bar{u}\rangle = \frac{u_*}{\kappa}\ln\left(\frac{z-d}{z_0}\right) \quad (10)$$

where κ is the von Kármán constant (= 0.4 in this paper) and z_0 the roughness length [54]. The friction velocity u_* is estimated by the turbulent momentum flux [39,43]. The roughness parameters d and z_0 are determined by the regression of the average velocity data with the log-law Equation (10). Table 1 tabulates the roughness parameters in which d and z_0 are in the range of $0.43h \leq d \leq 1.25h$ and $0.009h \leq z_0 \leq 0.047h$, respectively. Alike the turbulent boundary layer thickness, these values are comparable to those in the previous study measured over street canyons of AR = 1/2 ($d = 0.866h$ and $z_0 = 0.028h$) [51]. Higher values of d ($d > h$) are found in the cases of AR = 1/2 (Case L1 and Case H1 in Table 1) and 1/4 at low wind speed (Case L2). This feature is also observed in other studies [43,51], showing that the estimate to d could be higher than h by curve fitting.

It is worthy to look into several (dimensionless) ratios in the flows at low (3.3 m sec^{-1}) and high (6.6 m sec^{-1}) wind speeds to examine whether the dynamics are independent from Reynolds number (Table 1). The variations of u_*/U_∞, z_0/h and d/h are in the ranges of 1.8% to 4.5%, 14% to 42% and 9% to 21%, respectively. We therefore find that most cases are quite independent from Reynolds number except the one of AR = 1/4. The variation in u_*/U_∞ is small (4.5%) but large variations are found in z_0/h (42%) and d/h (21%) so it is hard to confirm Reynolds-number independence for AR = 1/4. The reason is likely attributed to the uncertainty of determining z_0 and d by the regression of measured wind speed profile to the log-law in the ISL where the turbulent momentum flux is assumed to be rather constant (less than 10% spatial variation). Additional wind-tunnel experiments (with higher wind speeds) are thus needed in the future studies. Analogous to the dimensionless ratio z_0/h, the Jensen number Je (= h/z_0) is a primary scaling quantity commonly employed in wind engineering. It is in the range of $20 \leq Je \leq 110$ whose variation between the cases of low and high wind speeds is about 3% to 20%.

Noticeable differences are observed in the fluctuating wind components over different rough surfaces at different freestream wind speeds. For instance, fluctuating streamwise velocity $\langle \overline{u'u'} \rangle^{1/2}$ (Fig. 2b), fluctuating vertical velocity $\langle \overline{w'w'} \rangle^{1/2}$ (Fig. 2c) and turbulent momentum flux $\langle \overline{u'w'} \rangle$ (Fig. 2d). These findings suggest that the near-wall turbulence structure is strongly affected by the (shear or form) drag induced by the roughness elements so is the transport processes

[39]. We hypothesize the analogy of pollutant plume dispersion which is elaborated in Section 4.2. *Pollutant dispersion*. The fluctuating components are normalized by the freestream wind speed so scaling similarity is observed mainly in the outer region $z \geq 0.5\delta$. Given the same freestream wind speed, the intensities of various fluxes generally increase with decreasing AR (widening street width). Moreover, the profiles over the array of street canyons of AR = 1/8 overlap with those of AR = 1/12, suggesting that peaked turbulent momentum flux appears when the building spacing is wide enough. Whereas, the near-wall fluctuating streamwise velocity for AR = 1/4 is slightly over its AR = 1/12 counterpart. Further experiments are thus needed to look into that regard. It is noted that the vertical profiles of flows over the array of street canyons of AR = 1/12 are mainly measured above the streets while others are measured above both streets and buildings (Fig. S1 of the Supplementary Material). This sampling limitation would overestimate the near-wall turbulent fluxes 10% to 20% at most [39].

Comparing the fluctuating velocities measured at the two different freestream wind speeds shows that the dimensionless profiles collapse well for $\left\langle \overline{u'u'} \right\rangle^{1/2}$ but differences are observed in those of $\left\langle \overline{w'w'} \right\rangle^{1/2}$ and $\left\langle \overline{u'w'} \right\rangle$. The differences are more notable over rougher surfaces of larger skin friction coefficient (wider street width) in the near-wall region. It is probably because the friction-velocity-to-freestream-wind-speed ratio u_*/U_∞ is larger in the tests with a higher freestream wind speed $U_\infty \approx 6.6$ m sec^{-1}, leading to elevated fluctuating velocity components. The difference (at most 20%) in the vertical fluctuating velocity $\left\langle \overline{w'w'} \right\rangle^{1/2}$ and the turbulent momentum flux $\left\langle \overline{u'w'} \right\rangle$ among the wind-tunnel measurements at different freestream wind speeds diminishes for $z \geq 0.5\delta$. The scale similarity is fulfilled only in the outer region because the freestream wind speed is not the best characteristic velocity scale for the near-wall flows where the dynamics are shear dominated. The scale dependence on shear using friction velocity u_* is elaborated below.

Fig. 3 depicts the vertical profiles of wind velocity $\left\langle \overline{u} \right\rangle$ normalized by the friction velocity u_* that is expressed in term of the dimensionless wall-normal distance $(z - d)/z_0$ over different rough surfaces in logarithmic scale. All the profiles, regardless of the freestream wind speed U_∞, clearly exhibit the conventional log-law behavior, demonstrating that the ISL is well developed in our wind tunnel measurements. The ISLs for flows over the array of street canyons of AR = 1/2 locate much higher that are followed by their AR = 1/4, 1/8 and 1/12 counterparts (increasing aerodynamic resistance). The diversified near-wall average velocities are induced by the roughness sublayer (RSL) dynamics where the aerodynamic resistance is amplified, further slowing down the flows. The average wind profiles over arrays of street canyons of ARs = 1/8 and 1/12 overlap closely with each other because the aerodynamic resistance is dominated by the form drag (or flow impingement) across individual roughness elements when their separation is wide enough (prevailing flows entrain down to the street level). The difference among the cases with different freestream wind speeds U_∞ is small (at most 5%) because the Reynolds number Re_∞ is sufficiently high for fully developed flows (Table 1).

4.2. Pollutant dispersion

Vertical profiles of mean concentration are measured at different streamwise locations x after the line source. As observed in the laboratory, the plume spreads gradually in the streamwise direction (Fig. S2). Fig. 4 illustrates the self-similar vertical dimensionless profiles of pollutant concentrations over arrays of street canyons of ARs = 1/2, 1/4, 1/8 and 1/12. The wall-normal distance is normalized by the dispersion coefficient

$$\sigma_z(x) = \left[\frac{\int_h^\delta z^2 \times \overline{\psi}(x,z)\, dz}{\int_h^\delta \overline{\psi}(x,z)\, dz} \right]^{1/2} \tag{11}$$

while the pollutant concentration is normalized by its canopy-level value

$$\overline{\psi}_{\mathrm{canopy}}(x) = \overline{\psi}(x, z=h) = \sqrt{\frac{2}{\pi}} \times \frac{Q}{U\sigma_z(x)}. \tag{12}$$

This approach helps focus on the dynamics within plume coverage. Although it is not the maximum, the canopy-level pollutant concentration is an appropriate characteristic scale for normalization. Unlike the maximum concentration, $\overline{\psi}_{\mathrm{canopy}}$ is independent from the elevation z.

that can be derived analytically. The vertical dimensionless profiles of concentration $\overline{\psi}(x,z)/\overline{\psi}_{\text{canopy}}(x)$ measured in different streamwise positions x, regardless of freestream wind speeds U_∞, collapse well with each other that fit into the theoretical Gaussian distribution Equation (2). It is hence suggested that ASL pollutant plume dispersion over rough surfaces, such as urban areas, exhibits the conventional Gaussian form similar to its ABL counterpart. A notable elevation of vapor concentration is observed in the near-wall region ($z \leq 0.75 \times 2^{1/2}\,\sigma_z$). This peaked concentration is mainly attributed to the flows over the windward wall of roughness elements where the sharp edges (singularities) enhance the local turbulence levels that in turn dilute the tracer adjacent to solid boundaries. This phenomenon was also reported by previous studies [4,19,23]. The sharp mean-wind-speed gradient over rough surfaces transports pollutants by advection in a non-uniform manner. Moreover, the (vertical) discharge momentum at the ground level line source induces initial plume rise that ends up in elevated concentration peak in the near-wall region. Although the uncertainty is not large, additional tests for the sensitivity of plume trajectory and tracer distribution to the source-level discharge momentum will be performed to confirm the findings in this paper and the uncertainty induced by imperfect experimental setting. Another possible reason is that the water vapor condenses on the (cooler) aluminum rib surfaces. It subsequently reduces canopy-level tracer concentrations and eventually raises the dimensionless tracer concentrations aloft. Besides, Fig. 4a compares the vertical dimensionless profiles of tracer concentrations over the array of street canyons of AR = 1/2 between this study and Salizzoni et al. [24]. The plume core converges to the theoretical Gaussian distribution. Comparing the Gaussian profiles and wind tunnel measurements, the coefficient of determination R^2 is over 0.95 and the root-mean-square (RMS) error is less than 0.2 so their agreement is favorable. Instead of the roof-level concentration $\overline{\psi}_{\text{canopy}}$, MacDonald et al. [4] used the (elevated) peak concentration in the normalization in which their coefficient of determination is similar to ours but the RMS error is slightly improved. Nonetheless, we suggest to use the roof-level concentration and the Gaussian model in the normalization in this paper because of the solid theoretical basis. Alternatives will be tested in future studies.

Fig. 5 attempts to characterize the tracer plume dispersion over hypothetical urban areas of different aerodynamic resistance by comparing the dimensionless profiles of vertical dispersion coefficient σ_z at different streamwise locations x, skin-friction coefficient c_f and freestream wind speeds U_∞. The vertical dispersion coefficient σ_z increases with increasing streamwise distance x because of crosswind turbulent transport together with widening plume coverage. A good fit of power regression is obtained (coefficient of determination $0.980 \leq R^2 \leq 0.995$) for all the cases of low (Fig. 5a) and high (Fig. 5b) wind speeds in which the regression power is in the range of $0.39 \leq n \leq 0.47$ (Table 2). The value of n obtained in this paper is smaller ($\leq$ 25%) than the theoretical one (n = 0.5) commonly used in the Gaussian plume models in isothermal conditions in far field [5]. The smaller values of power n observed in the current wind tunnel measurements are mainly attributed to the under estimate of σ_z in the far field ($x \geq 37.5h$) because of vapor condensation in the near-wall region (Fig. 5). The power n of σ_z regression from the LES of Wong and Liu [7] is higher ($0.52 \leq n \leq 0.66$) and of Ng and Liu [55] is lower ($0.40 \leq n \leq 0.58$). Deviations of the mathematical modeling results are probably caused by inaccurate boundary conditions and coarse spatio-temporal resolution. The value of n (= 0.69) over an array of street canyons of AR = 1/2 from the wind tunnel results of Salizzoni et al. [24] is even higher. The discrepancy could be attributed to the different (background) turbulence levels and/or modeling parameters in various studies. Moreover, addition of small roughness elements at the top of the bars enhanced the turbulent fluxes that would further enlarge the dispersion coefficient. Nonetheless, the value of power n obtained in this study is comparable to that of other studies and it generally falls into a reasonable range.

The vertical dispersion coefficients σ_z measured over different rough surfaces do not converge onto a universal function of streamwise distance x, demonstrating that crosswind plume dispersion also depends on the surface roughness (Fig. 5). The plume spreads in the isolated roughness regime (ARs = 1/8 and 1/12) and wake interference regime (AR = 1/4) are obviously wider than that in the skimming-flow regime (AR = 1/2) in both U_∞ = 3.3 m sec^{-1} (Fig. 5a) and U_∞ = 6.6 m sec^{-1} (Fig. 5b). It is noteworthy that, within the isolated roughness regime, the plume spread over the arrays of street canyons of ARs = 1/8 and 1/12 is similar. Its coverage is even narrower with further increase in street width (decreasing AR) in the 3.3-m-sec^{-1} dataset. This feature is analogous to that of skin-friction coefficient c_f, suggesting the possible relation between the two parameters. Moreover, Salizzoni et al. [24] reported that, with increasing aerodynamic resistance (from AR = 1 to 1/2), turbulent mixing is enhanced that in turn enlarges the plume coverage. Using LES, Wong and Liu [7] showed that the vertical dispersion coefficient σ_z initially increases with decreasing AR (skimming flow regime), reaches a peak at AR = 1/10 (wake interference regime) then decreases thereafter with further decrease in AR (isolated roughness regime). These findings are generally in line with those available in literature.

4.3. Dependence of plume spread on aerodynamic resistance

In most pollutant plume dispersion theory, vertical dispersion coefficient σ_z can be expressed as a function of streamwise distance x

$$\sigma_z = Ax^n \tag{13}$$

where A and n are empirical constants. Neither A nor n consider the effects of aerodynamic resistance over urban areas in the conventional Gaussian plume dispersion theory. Given the different turbulence-generation mechanism in isothermal ASLs and thermally stratified ABLs, the skin-friction coefficient c_f of hypothetical urban areas is introduced to handle the influence of surface roughness and blockage orientation on the dynamics in term of σ_z. The skin-friction coefficient deduced from the extrapolation of vertical profiles of turbulent momentum flux measured in different streamwise locations increases with decreasing AR, reaches the maximum at AR = 1/8 and decreases thereafter for both measurements in freestream wind speeds U_∞ = 3.3 m sec^{-1} and 6.6 m sec^{-1} (Table 1). This feature is similar to the numerical results using LES [56] and Reynolds-averaged Navier-Stokes (RANS) turbulence models [38,57] in which a plateau of skin-friction coefficient over surface configurations close to AR = 1/8 was clearly shown. Alike its skin-friction coefficient counterpart, the vertical dispersion coefficient σ_z for tracer plume dispersion over arrays of street canyons is peaked at AR = 1/8 though the results over arrays of street canyons of ARs = 1/8 and 1/12 are very close to each other in freestream wind speed U_∞ = 6.6 m sec^{-1}. This is mainly because the turbulent velocities are similar between these two surface configurations (Fig. 1).

Section 2. Theoretical background derives analytically the vertical dispersion coefficient σ_z as a function in terms of the downwind distance measured from the pollutant source x, the turbulent boundary layer thickness δ and the skin-friction coefficient c_f i.e. Equation (6) $\sigma_z \propto x^{1/2}\times\delta^{1/2}\times c_f^{1/4}$. Most existing studies available in literature used n = 0.5. To verify the analytical hypothesis, the vertical dispersion coefficient σ_z is plotted against the newly proposed friction length scale L_f (= $x^{1/2}\times\delta^{1/2}\times c_f^{1/4}$; Fig. 6). The length dimensions (σ_z, x and δ) are normalized by the size of roughness elements h. The vertical dispersion coefficient is almost directly proportional to the friction length scale $\sigma_z \propto L_f$. The nonzero σ_z ($\approx$ 0.4 h) at L_f = 0 is caused by the lifting of effective source height and the x offset due to the physical width of the line source. Scale similarity is clearly demonstrated even the data are collected in different freestream wind speeds. Linear regression shows that there is a close relation between σ_z and L_f (coefficient of determination by liner regression R^2 = 0.93). This analytical formulation thus could be used in the future parameterization of pollutant plume dispersion over urban areas to handle complicated building roughness in isothermal conditions.

5. Conclusion

This paper first reports the use of water vapor to study the pollutant plume dispersion over hypothetical urban areas in laboratory-scale wind tunnel experiments. The tracer concentrations over arrays of street canyons exhibit the conventional Gaussian distribution that are compared favorably with those in previous studies. It is hence suggested the feasibility of using water vapor as an affordable and harmless tracer in wind tunnel experiments. The analytical derivation and empirical solution collectively suggest an improved parameterization of pollutant plume dispersion coefficient over rough surfaces using skin friction coefficient ($8\times10^{-3} \le c_f \le 13\times10^{-3}$).

The (maximum) difference in the concentrations between wind-tunnel experiments and Gaussian model is up to 10% to 20% that is mainly attributed to the non-uniform mean wind speed and discharge momentum from the ground-level line source, which, however, do not exist in idealized configuration. Although the discrepancy is not negligible, the simplicity, user-friendliness and cost-effectiveness of the Gaussian-model framework are attractive benefits from the end-users' perspective solving practical engineering problems. The current parameterization might case up to 20% underestimation of the peaked pollutant concentration. Nonetheless, studies of rectification, such as including the non-zero plume trajectory, are currently undertaken to improve the accuracy of the parameterization.

We note the rather narrow range of boundary layer thickness ($12h \le \delta \le 15h$) tested in this paper. It is attributed to the use of identical roughness elements in the wind tunnel experiments. As a preliminary study, more conservative roughness elements are employed in order to maintain the homogeneity in the horizontal extent. After earned a basic understanding, more diversified roughness-element types, source configurations and flows conditions should be performed to further verify the newly developed parameterization of (vertical) dispersion coefficient. The current wind tunnel experiments are conducted in the isothermal conditions. In view of the different turbulence generation mechanism, the newly developed parameterization must be applied cautiously in case stable or unstable atmospheric stratification is considered.

Only 2D ribs in crossflows are adopted in this paper, which, however, are seldom found in realistic urban areas. The lack of representation would reduce the functionality of our work. Besides, prevailing wind direction normal to the street axes is only one of the many scenarios. Deviation from the normal wind would change the flows substantially that might weaken the conclusions arrived in this paper. More roughness elements of different shape and geometry are therefore needed to verify our newly developed parameterization.

Apart from the aforementioned limitation, future studies will focus on the validation of the analytical and empirical solutions in a systematic manner. The major benefit of the newly developed parameterization, i.e. use the simple skin-friction coefficient c_f instead of the complicated urban morphology in terms of floor plan, obstacle blockage and building orientation, etc., to model the effect of rough urban surfaces on pollutant plume dispersion by non-computational-fluid-dynamics (non-CFD) air quality impact assessment.

Acknowledgements

We would like to thank the anonymous reviewers for their invaluable suggestion for the improvement of the manuscript. This study is supported by the General Research Fund (GRF) 17205314 of the Hong Kong Research Grants Council (RGC). The technical support from Mr. Vincent K.W. Lo as well as the setup of wind tunnel infrastructure by Dr. Yat-Kiu Ho are appreciated.

Manuscript word count: 6,800

(Including text, figure captions and table legends, but not references).

References

[1] B.R. Gurjar; T.M. Butler, M.G. Lawrence, J. Lelieveld, Evaluation of emissions and air quality in megacities, *Atmos. Environ. 42 (2008)* 1593-1606.

[2] C.H. Liu, D.Y.C. Leung, M.C. Barth, On the prediction of air and pollutant exchange rates in street canyons of different aspect ratios using large-eddy simulation, *Atmos. Environ. 39 (2005)*, 1567-1574.

[3] M.R. Raupach, R.A. Antonia, S. Rajagopalan, Rough-wall turbulent boundary layers, *Appl. Mech. Rev. 44 (1991)* 1-25.

[4] R.W. MacDonald, R.F. Griffiths, D.J. Hall, A comparison of results from scaled field and wind tunnel modelling of dispersion in arrays of obstacles, *Atmos. Environ. 32 (1998)* 3845-3862.

[5] N. de Nevers, *Air Pollution Control Engineering*, Waveland Press, 2010.

[6] D.B. Turner, *Workbook of Atmospheric Dispersion Estimates: an Introduction to Dispersion Modeling*, Lewis Publishers, London, 1994.

[7] C.C.C. Wong, C.H. Liu, Pollutant plume dispersion in the atmospheric boundary layer over idealized urban roughness, *Bound.-Layer Meteor. 147 (2013)* 281-300.

[8] F. Pasquill, F.B. Smith, *Atmospheric Diffusion*, 3rd, ed. Wiley, New York, 1983.

[9] M.J. Davidson, K.R. Mylne, C.D. Jones, J.C. Phillips, R.J. Perkins, J.C.H Fung, J.C.R. Hunt, Plume dispersion through large groups of obstacles—A field investigation, *Atmos. Environ. 29 (1995)* 3245-3256.

[10] R.E. Britter, S.R. Hanna, Flow and dispersion in urban areas, *Annu. Rev. Fluid. Mech. 35(2003)* 469-496.

[11] J. Jiménez, Turbulent flows over rough walls. *Annu. Rev. Fluid. Mech. 36 (2004)* 173-196.

[12] C. Gromke, A vegetation modeling concept for building and environmental aerodynamics wind tunnel tests and its application in pollutant dispersion studies. *Environ. Pollut.* 159, (2011) 2094-2099.

[13] W.H. Snyder, *Guideline for Fluid Modeling of Atmospheric Diffusion*, Report No. 600/8-81-009, USEPA, Research Triangle Park, NC 27711, 1981.

[14] X.X. Li, D.Y.C. Leung, C.H. Liu, K.M. Lam, Physical modeling of flow field inside urban street canyons, *J. Appl. Meteorol. Climatol*. 47 (2008) 2058-2067.

[15] S. Pournazeri, M. Princevac, A. Venkatram, Rise of buoyant emissions from low-level sources in the presence of upstream and downstream obstacles, *Bound.-Layer Meteorol. 144* (2012) 287-308.

[16] P.Y. Cui, Z. Li, W.Q. Tao, Wind-tunnel measurements for thermal effects on the air flow and pollutant dispersion through different scale urban areas. *Build. Environ.* 97 (2016) 137-151.

[17] B. Hajra, T. Stathopoulos, A. Bahloul, The effect of upstream buildings on near-field pollutant dispersion in the built environment. *Atmos. Environ.* 45 (2011) 4930-4940.

[18] B. Hajra, T. Stathopoulos, A wind tunnel study of the effect of downstream buildings on near-field pollutant dispersion. *Build. Environ.* 52 (2012) 19-31.

[19] A.H. Huber, Wind tunnel and Gaussian plume modeling of building wake dispersion, *Atmos. Environ. 25* (1991) 1237-1249.

[20] B. Hajra, T. Stathopoulos, A. Bahloul, Assessment of pollutant dispersion from rooftop stacks: ASHRAE, ADMS and wind tunnel simulation. *Build. Environ.* 45 (2010) 2768-2777.

[21] A. Gupta, T. Stathopoulos, P. Saathoff, Wind tunnel investigation of the downwash effect of a rooftop structure on plume dispersion. *Atmos. Environ.* 46 (2012) 496-507.

[22] Y. Tominaga, S.I. Akabayashi, T. Kitahara, Y. Arinami, Air flow around isolated gable-roof buildings with different roof pitches: Wind tunnel experiments and CFD simulations. *Build. Environ.* 84 (2015) 204-213.

[23] D.K. Heist, S.G. Perry, L.A. Brixey, A wind tunnel study of the effect of roadway configurations on the dispersion of traffic-related pollution, *Atmos. Environ. 43* (2009) 5101-5111.

[24] P. Salizzoni, R. Van Liefferinge, L. Soulhac, P. Mejean, R.J. Perkins, Influence of wall roughness on the dispersion of a passive scalar in a turbulent boundary layer, *Atmos. Environ. 43 (2009)* 734-748.

[25] G.A. Briggs, R.E. Britter, S.R. Hanna, J.A. Havens, A.G. Robins, W.H. Snyder, Dense gas vertical diffusion over rough surfaces: results of wind-tunnel studies, *Atmos. Environ. 35 (2001)* 2265-2284.

[26] J. Havens, H. Walker, T.O. Spicer, Wind tunnel study of air entrainment into two-dimensional dense gas plumes at the Chemical Hazards Research Center, *Atmos. Environ. 35* (2001) 2305-2317.

[27] W.H. Snyder, Wind-tunnel study of entrainment in two-dimensional dense-gas plumes at the EPA's fluid modeling facility, *Atmos. Environ. 35 (2001)* 2285-2304.

[28] S.G. Perry, D.K. Heist, L.H. Brouwer, E.M. Monbureau, L.A. Brixey, Characterization of pollutant dispersion near elongated buildings based on wind tunnel simulations, *Atmos. Environ. 142 (2016)* 286-295.

[29] S. Branford, O. Coceal, T.G. Thomas, S.E. Belcher, Dispersion of a point-source release of a passive scalar through an urban-like array for different wind directions, *Bound.-Layer Meteor. 139 (2011)* 367-394.

[30] C. Gromke, B. Blocken, Influence of avenue-trees on air quality at the urban neighborhood scale. Part II: Traffic pollutant concentrations at pedestrian level, *Environ. Pollut. 196 (2015)* 176-184.

[31] M. Lateb, R.N. Meroney, M. Yataghene, H. Fellouah, F. Saleh, M.C. Boufadel, On the use of numerical modelling for near-field pollutant dispersion in urban environments− A review, *Environ*. Pollut. 208 (2016) Part A, 271-283.

[32] Y. Zhang, K.C.S. Kwok, X.P. Liu, J.L. Niu, Characteristics of air pollutant dispersion around a high-rise building, *Environ. Pollut. 204 (2015)* 280-288.

[33] D.P. Chock, 1982. Pollutant dispersion near roadways — Experiments and modeling, *Sci. Total Environ. 25 (1982)* 111-132.

[34] R.W. MacDonald, R.F. Griffiths, S.C. Cheah, Field experiments of dispersion through regular arrays of cubic structures, *Atmos. Environ. 31 (1997)* 783-795.

[35] J. Pospisil, J. Katolicky, M. Jicha, A comparison of measurements and CFD model predictions for pollutant dispersion in cities, *Sci. Total Environ. 334-335 (2004)* 185-195.

[36] K.K. Leung, C.H. Liu, C.C.C. Wong, J.C.Y. Lo, G.C.T. Ng, On the study of ventilation and pollutant removal over idealized two-dimensional urban street canyons, *Build. Simul. 5 (2012)* 359-369.

[37] C.H .Liu, C.T. Ng, C.-T., Wong, C.C.C., 2015. A theory of ventilation estimate over hypothetical urban areas, *J. Hazard. Mater. 296*, 9-16.

[38] Y.K. Ho, C.H. Liu, M.S. Wong, Preliminary study of the parameterisation of street-level ventilation in idealised two-dimensional simulations, *Build. Environ. 89 (2015)* 345-355.

[39] Y.K. Ho, C.H. Liu, A wind tunnel study of flows over idealised urban surfaces with roughness sublayer corrections, *Theor. Appl. Climatol. (2016)* 1-16.

[40] Z.W. Mo, C.H. Liu, Laboratory study of passive-scalar plume dispersion over hypothetical urban roughness, *American Meteorological Society 97th Annual Meeting*, January 22 to 26, 2017, Seattle, USA.

[41] A.E. Perry, W.H. Schofield, P.N. Joubert, Rough wall turbulent boundary layers, *J. Fluid. Mech. 37 (1969)* 383-413.

[42] J.H. Spurk, *Fluid Mechanics*, Springer-Verlag, Berlin, Heidelberg, 1997.

[43] H. Cheng, I.P. Castro, Near wall flow over urban-like roughness, *Bound.-Layer Meteor. 104 (2002)* 229-259.

[44] A. Ploss, I.P. Castro, H. Cheng, H., The surface region of rough wall boundary layers. In Advances in Turbulence VIII, *Proceedings of the Eighth European Turbulence Conference*, Dopazo, C., Ed. International Center for Numerical Methods in Engineering, 2000, pp. 455-459.

[45] S.P. Arya, *Air Pollution Meteorology and Dispersion*, Oxford University Press: Cambridge, U.K, 1999.

[46] K.L. Calder, Some recent British work on the problems of diffusion in the lower atmosphere, *Proceedings of the US Technique Conference Air Pollution*, Vol. 787, McGraw- Hill, New York, 1952.

[47] R.E. Britter, S.R. Hanna, G.A. Briggs, A. Robins, Short-range vertical dispersion from a ground level source in a turbulent boundary layer, *Atmos. Environ. 37 (2003)* 3885-3894.

[48] T.R. Oke, Street design and urban canopy layer climate, *Energ. Buildings 11 (1988)* 103-113.

[49] A.E. Perry, K.L. Lim, S.M. Henbest, An experimental study of the turbulence structure in smooth-and rough-wall boundary layers, *J. Fluid Mech. 177 (1987)* 437-466.

[50] H. Bruun, Interpretation of a hot wire signal using a universal calibration law. *J. Phys. E. Sci. Instrum. 4 (1971)* 225.

[51] P. Salizzoni, L. Soulhac, P. Mejean, R.J. Perkins, Influence of a two-scale surface roughness on a neutral turbulent boundary layer, *Bound.-Layer Meteor. 127 (2008)* 97-110.

[52] P. Burattini, S. Leonardi, P. Orlandi, R. Antonia, Comparison between experiments and direct numerical simulations in a channel flow with roughness on one wall. *J. Fluid Mech.* 600 *(2008)* 403-426.

[53] S.B. Pope, *Turbulent Flows*, Cambridge University Press, Cambridge, U.K, 2000.

[54] P. Jackson, On the displacement height in the logarithmic velocity profile, *J. Fluid Mech.* 111 *(1981)* 15-25.

[55] C.T. Ng, C.H. Liu, Numerical simulations of street canyon ventilation and pollutant dispersion, *Int. J. Environ. Pollut. 55 (2014)* 167-173.

[56] T.N.H. Chung, C.H. Liu, On the mechanism of air pollutant removal in two-dimensional idealized street canyons: a large-eddy simulation approach, *Bound.-Layer Meteor. 148 (2013)* 241-253.

[57] J.J. Baik, J.J. Kim, On the escape of pollutants from urban street canyons, *Atmos. Environ. 36 (2002)* 527-536.

List of Tables

List of Figures

freestream wind speed $U_\infty = 6.6$ m sec^{-1}. Also shown is the theoretical Gaussian-form tracer concentrations (dark solid line).

Fig. 5. Dimensionless vertical dispersion coefficients σ_z/h in the streamwise direction x/h over arrays of street canyons of aspect ratios ARs = 1/2 (□); 1/4 (△); 1/8 (◇) and 1/12 (○) in freestream wind speed (a) $U_\infty = 3.3$ m sec^{-1} and (b) $U_\infty = 6.6$ m sec^{-1}. Also shown are the regressions by power-law fitting $\sigma_z = Ax^n$ (solid lines).

Fig. 6. Vertical dispersion coefficient σ_z plotted against friction length scale L_f ($= x^{1/2} \times \delta^{1/2} \times C_f^{1/4}$) in freestream wind speed $U_\infty = 3.3$ m sec^{-1} (◆) and $U_\infty = 6.6$ m sec^{-1} (●). Also shown is the linear regression (solid line) for all the data points (the coefficient of determination by liner regression $R^2 = 0.933$). Size of roughness elements h is used as the characteristic length scale.

Supplementary Material

Fig. S1 Measurement locations in streamwise direction.

Fig. S2. Vertical dimensionless profiles of pollutant concentrations $\overline{\psi}/\overline{\psi}_{\text{canopy}}$ plotted against wall-normal distance $(z-h)/h$ at different streamwise locations x/h over arrays of street canyons of aspect ratios ARs = 1/2 (□); 1/4 (△); 1/8 (◇) and 1/12 (○) in freestream wind speed $U_\infty = 3.3$ m sec^{-1}. Filled symbols are the corresponding quantities in $U_\infty = 6.6$ m sec^{-1}.

Table 1. Configuration of the models of hypothetical urban areas and the flows in the wind tunnel experiments.

Measurement cases		Low Wind Speed ($U_\infty \approx 3.3$ m sec^{-1})				High Wind Speed ($U_\infty \approx 6.6$ m sec^{-1})			
		Case L1	Case L2	Case L3	Case L4	Case H1	Case H2	Case H3	Case H4
Aluminum rib [mm]	Size h	19	19	19	19	19	19	19	19
	Separation b	38	76	152	228	38	76	152	228
Aspect ratio AR (= h/b)		1/2	1/4	1/8	1/12	1/2	1/4	1/8	1/12
Boundary layer thickness δ [mm]		240	260	285	265	245	265	285	260
Wind speed [m sec^{-1}]	Freestream U_∞	3.3	3.3	3.3	3.3	6.7	6.6	6.7	6.6
Friction velocity [m sec^{-1}]	u_*	0.18	0.22	0.22	0.22	0.38	0.45	0.47	0.47
	u_*/U_∞	0.056	0.065	0.068	0.068	0.057	0.068	0.071	0.071
Skin-friction coefficient	Minimum	7.3	10	12	11	7.8	11	11	12
[$\times 10^{-3}$]	Mean	8.0	10	12	12	8.4	11	13	13
c_f (= $2u_*^2/U_\infty^2$)	Maximum	8.5	11	13	13	8.8	12	14	14
Reynolds number	Re_∞ (= $U_\infty\delta/\nu$)	79	86	93	84	160	180	190	170
[$\times 10^3$]	Re_* (= $u_*\delta/\nu$)	4	6	6	6	9	12	14	12
Displacement height	d/h	1.13	1.04	0.48	0.81	1.25	0.84	0.43	0.74
Roughness length	z_0/h	0.009	0.017	0.041	0.032	0.011	0.026	0.047	0.038
Jensen number	Je (= h/z_0)	110	59	24	31	91	38	21	26

Remark: L and H denote the cases in low wind speed ($U_\infty \approx 3.3$ m sec^{-1}) and high wind speed ($U_\infty \approx 6.6$ m sec^{-1}), respectively. The skin-friction coefficient c_f is rounded to two significant figures.

Table 2. Power n of the power-law fitting measured in different settings.

Aspect ratio	Salizzoni et al. [24]	Wong and Liu [7]	Ng and Liu [55]	Current study	
				Low wind speed ($U_\infty \approx 3.3$ m sec^{-1})	High wind speed ($U_\infty \approx 6.6$ m sec^{-1})
1/2	0.69	0.66	0.40	0.42	0.47
1/4	---	0.52	0.43	0.41	0.39
1/8	---	0.54	0.48	0.41	0.41
1/12	---	0.56	0.58	0.45	0.47

Remark: Power-law fitting $\sigma_z = Ax^n$.

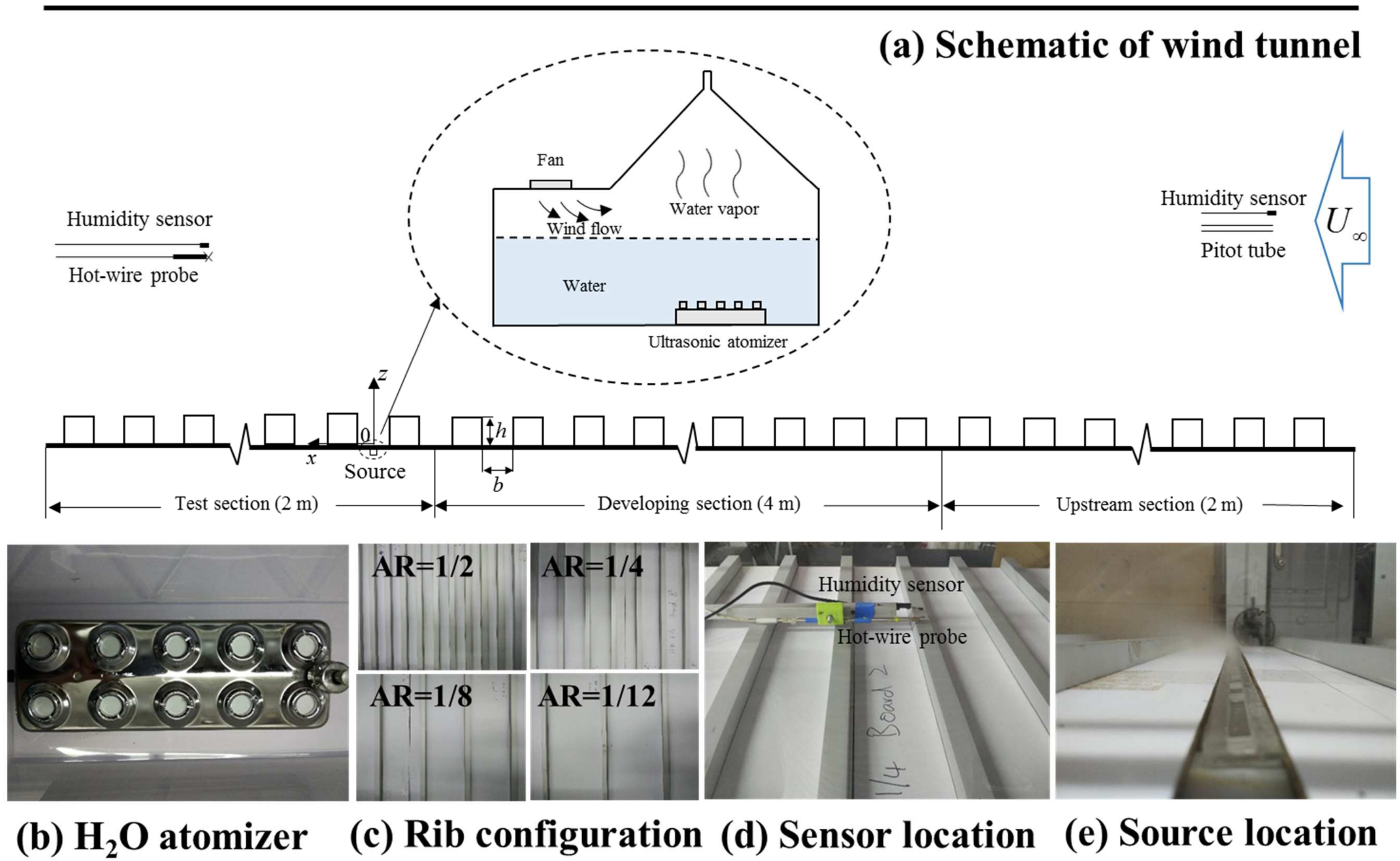

Fig. 1. Schematic of wind tunnel setup, rough surface configuration and source design. For visualization purposes, moisture emission is captured in Fig. 1 (e). In the experiments, only water vapor is emitted from the ground-level line source by the water atomizer.

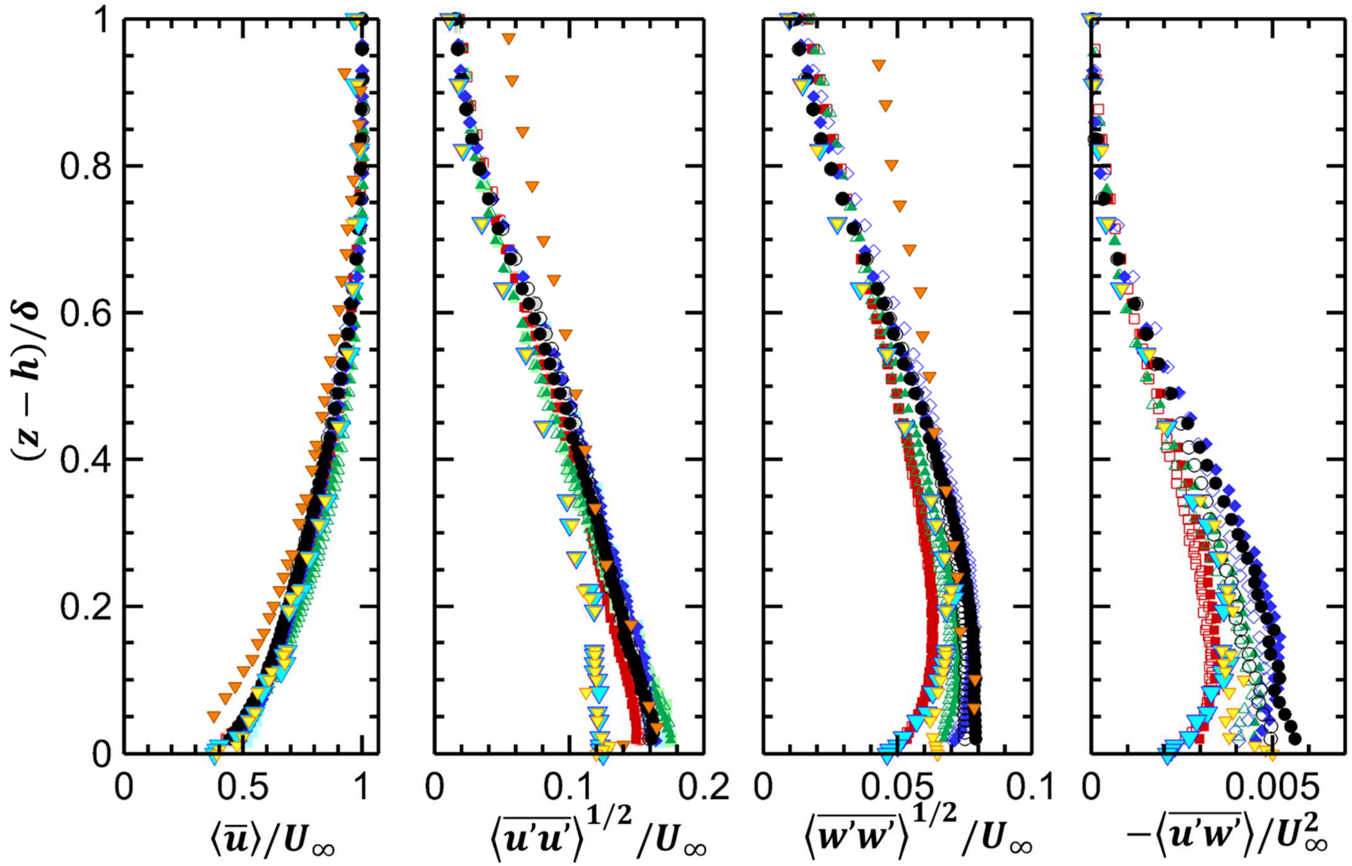

Fig. 2. Vertical dimensionless profiles of flow variables plotted against wall-normal distance $(z-h)/\delta$ over arrays of street canyons of aspect ratios ARs = 1/2 (□); 1/4 (△); 1/8 (◇) and 1/12 (○) in freestream wind speed U_∞ = 3.3 m sec^{-1}. Filled symbols are the corresponding quantities in U_∞ = 6.6 m sec^{-1}. Also shown are the wind tunnel data available from literature: AR = 1/2 roof top (▼) [51], AR = 1/2 cavity top (▼) [51] and AR = 1/3 (▼) [52].

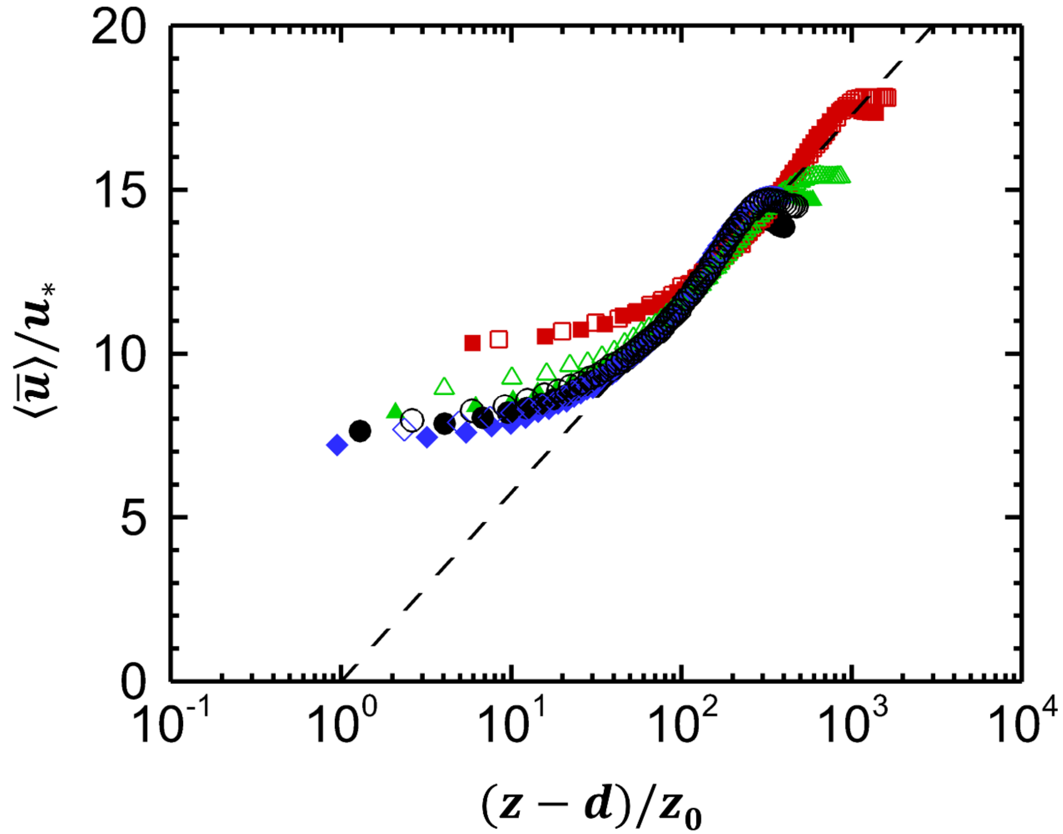

Fig. 3. Vertical dimensionless profiles of mean velocity $\langle\bar{u}\rangle/u_*$ plotted against wall-normal distance $(z - d)/z_0$ over arrays of street canyons of aspect ratios ARs = 1/2 (□); 1/4 (△); 1/8 (◇) and 1/12 (○) in freestream wind speed U_∞ = 3.3 m sec^{-1}. Filled symbols are the corresponding quantities in U_∞ = 6.6 m sec^{-1}. Also shown is the conventional logarithmic law of the wall (log-law) Equation (10) (dashed line).

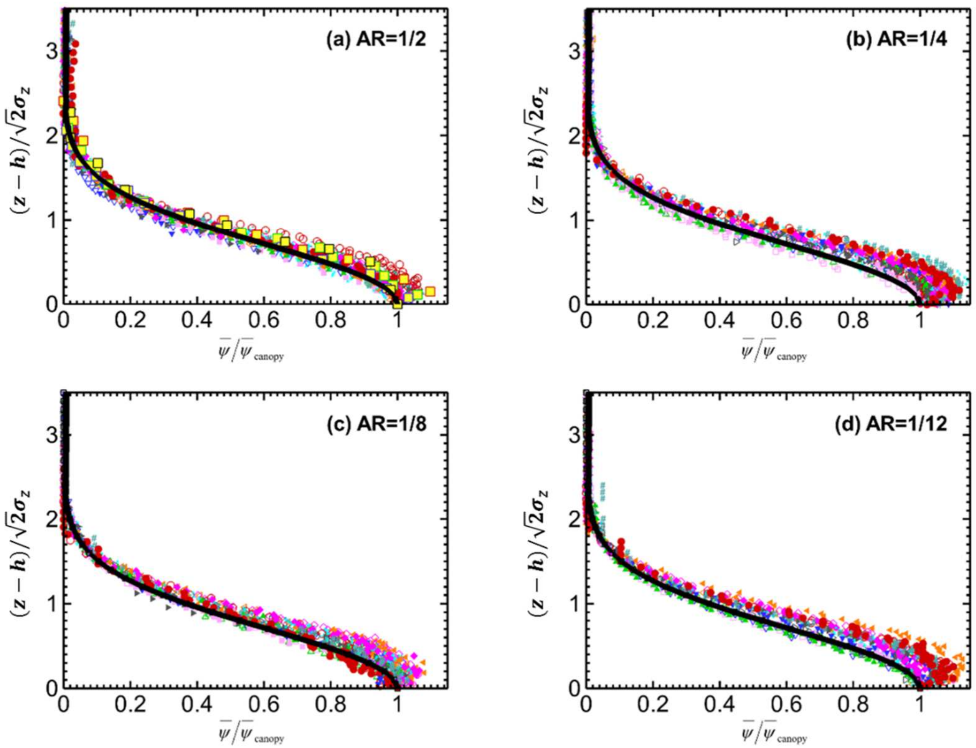

Fig. 4. Vertical dimensionless profiles of tracer concentrations $\overline{\psi}/\overline{\psi}_{\text{canopy}}$ plotted against wall-normal distance $(z-h)/2^{1/2}\sigma_z$ over arrays of street canyons of aspect ratios ARs = (a) 1/2; (b) 1/4; (c) 1/8 and (d) 1/12 at x = 10h (□); 15h (△); 22.5h(▽); 30h (▷); 37.5h (◁); 45h (◇); 52.5h (+); 60h (-) and 67.5h (○) in freestream wind speed U_∞ = 3.3 m sec^{-1}. Filled symbols are the corresponding quantities in U_∞ = 6.6 m sec^{-1}. Yellow-filled symbols are the wind tunnel results of Salizzoni et al. [23] at x = 9h (□); 15h (□). 22.5h (□) and 30h (□) in freestream wind speed U_∞ = 6.6 m sec^{-1}. Also shown is the theoretical Gaussian-form tracer concentrations (dark solid line).

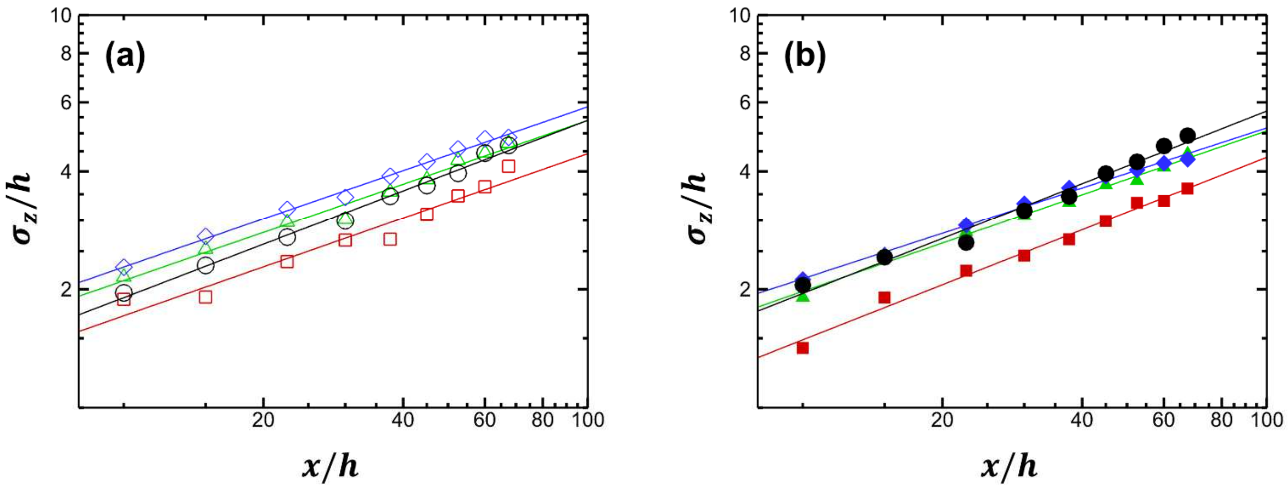

Fig. 5. Dimensionless vertical dispersion coefficients σ_z/h in the streamwise direction x/h over arrays of street canyons of aspect ratios ARs = 1/2 (□); 1/4 (△); 1/8 (◇) and 1/12 (○) in freestream wind speed (a) $U_\infty = 3.3$ m sec^{-1} and (b) $U_\infty = 6.6$ m sec^{-1}. Also shown are the regressions by power-law fitting $\sigma_z = Ax^n$ (solid lines).

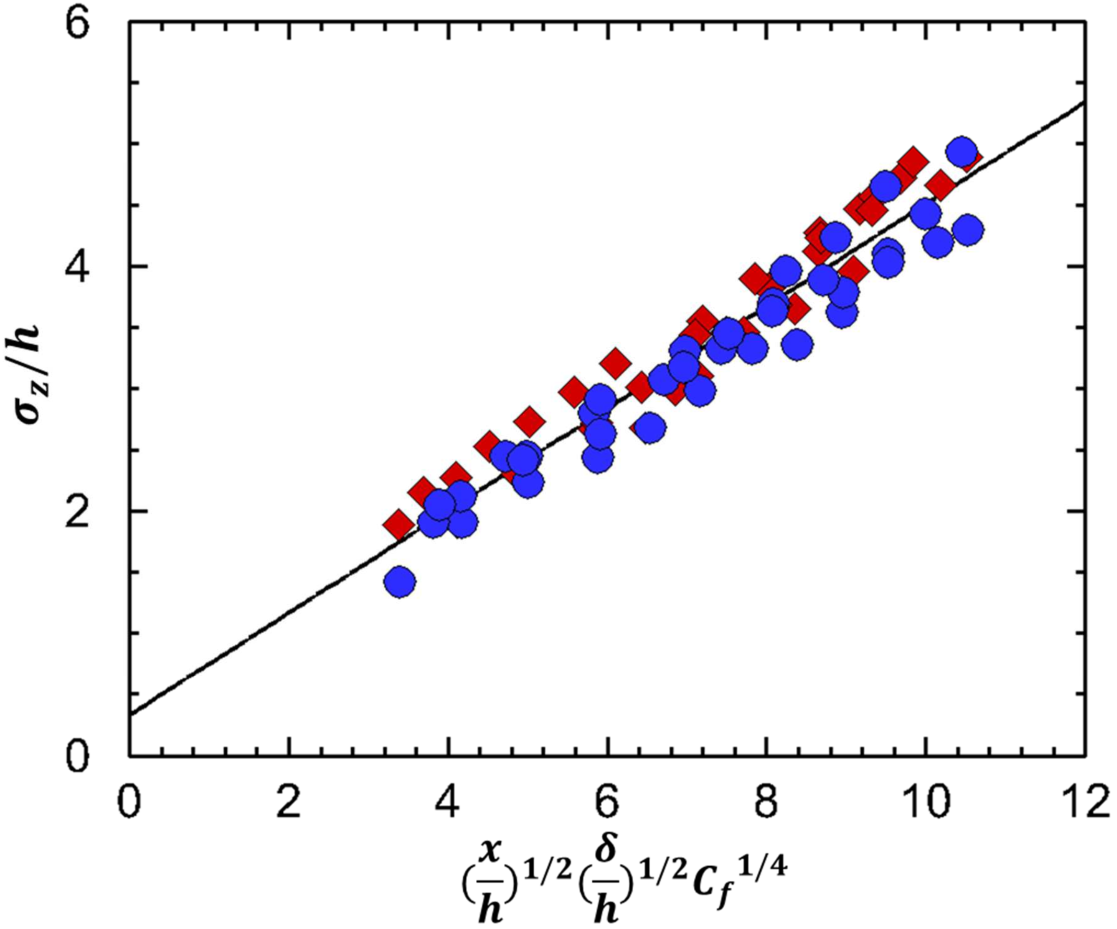

Fig. 6. Vertical dispersion coefficient σ_z plotted against friction length scale L_f (= $x^{1/2}\times\delta^{1/2}\times C_f^{1/4}$) in freestream wind speed U_∞ = 3.3 m sec^{-1} (◆) and U_∞ = 6.6 m sec^{-1} (●). Also shown is the linear regression (solid line) for all the data points (the coefficient of determination by liner regression R^2 = 0.933). Size of roughness elements h is used as the characteristic length scale.

Supporting Information

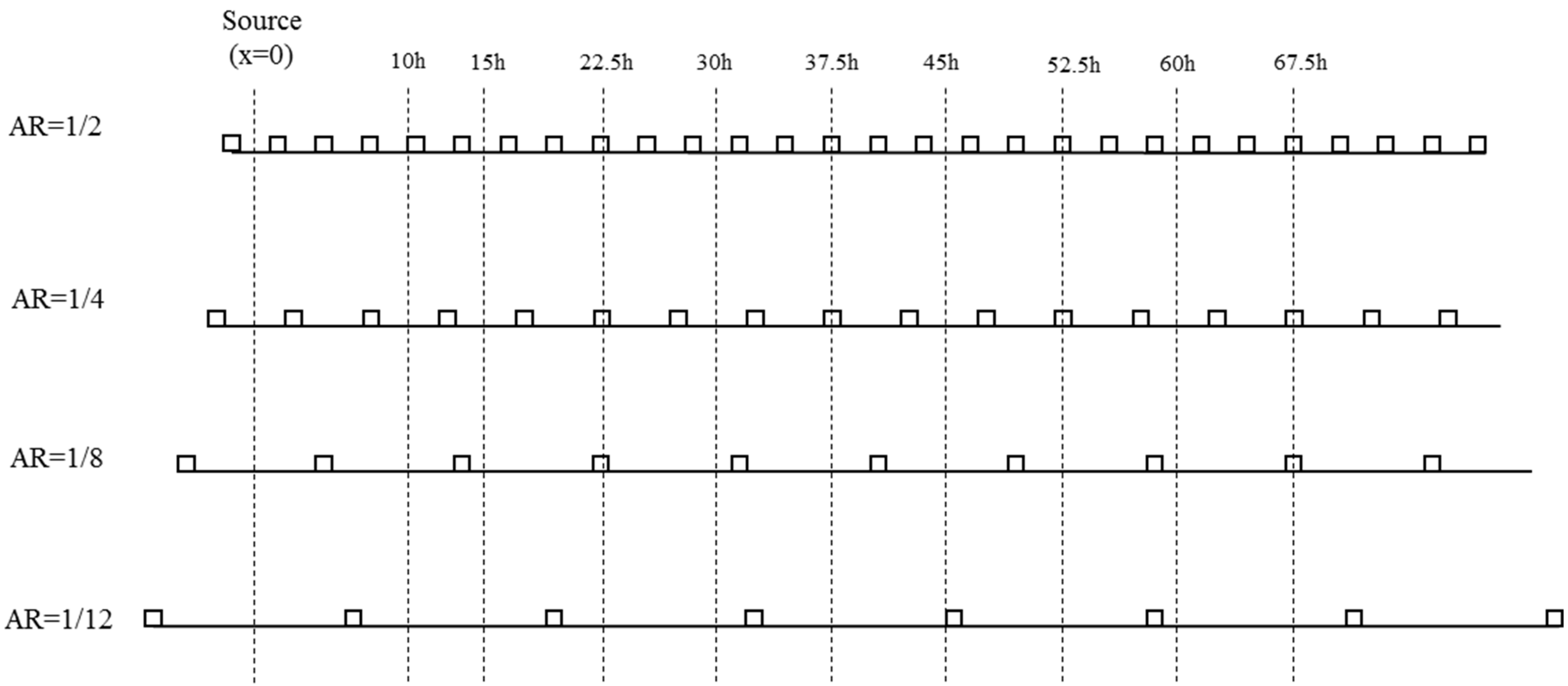

Fig. S1 Measurement locations in streamwise direction.

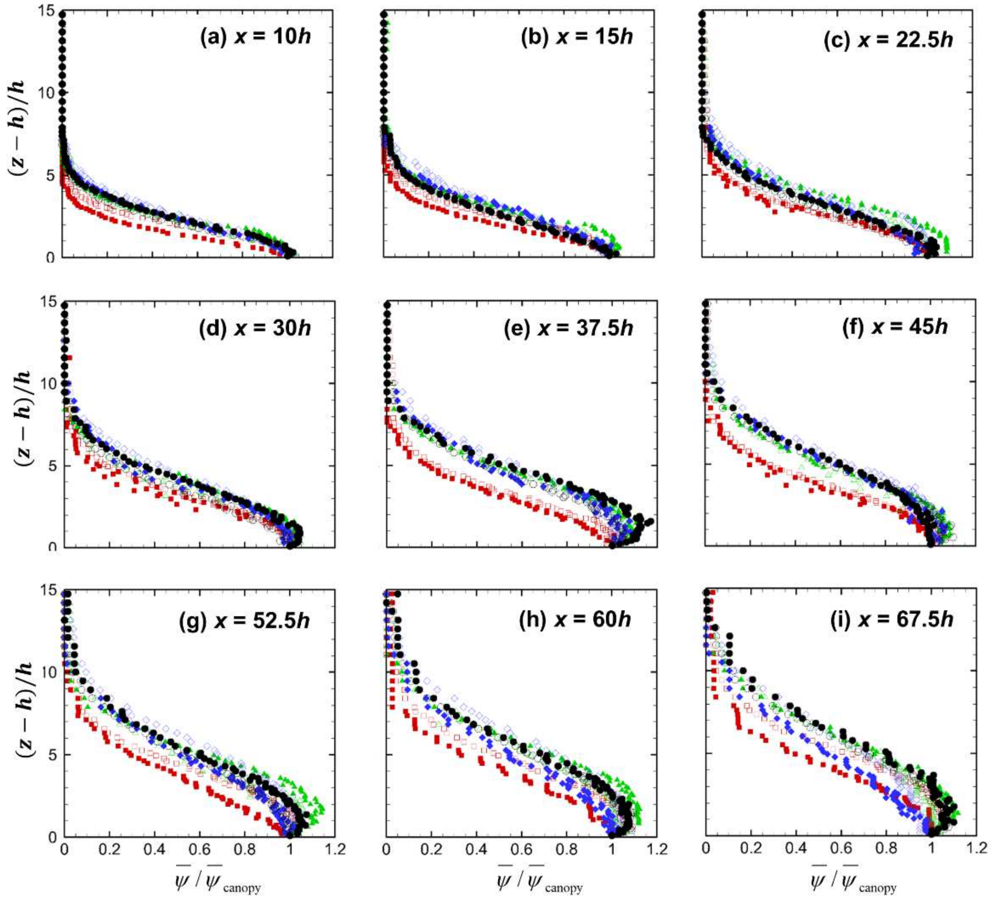

Fig. S2. Vertical dimensionless profiles of pollutant concentrations $\overline{\psi}/\overline{\psi}_{\text{canopy}}$ plotted against wall-normal distance $(z\text{-}h)/h$ at different streamwise locations x/h over arrays of street canyons of aspect ratios ARs = 1/2 (□); 1/4 (△); 1/8 (◇) and 1/12 (○) in freestream wind speed $U_\infty = 3.3$ m sec^{-1}. Filled symbols are the corresponding quantities in $U_\infty = 6.6$ m sec^{-1}.